Phonon-assisted Kondo effect in a single-molecule transistor out of equilibrium

2006 J. Phys.: Condens. Matter 18 5435

(http://iopscience.iop.org/0953-8984/18/23/015)

INSTITUTE OF PHYSICS PUBLISHING JOURNAL OF PHYSICS: CONDENSED MATTER

J. Phys.: Condens. Matter **18** (2006) 5435–5446 doi:10.1088/0953-8984/18/23/015

Phonon-assisted Kondo effect in a single-molecule transistor out of equilibrium

Zuo-Zi Chen[1], **Haizhou Lu**[1], **Rong Lü**[1] **and Bang-fen Zhu**[1,2]

[1] Center for Advanced Study, Tsinghua University, Beijing 100084, People's Republic of China
[2] Department of Physics, Tsinghua University, Beijing 100084, People's Republic of China

E-mail: zzchen@castu.tsinghua.edu.cn and bfzhu@castu.tsinghua.edu.cn

Received 24 February 2006
Published 26 May 2006
Online at stacks.iop.org/JPhysCM/18/5435

Abstract

The joint effect of the electron–phonon interaction and Kondo effect on nonequilibrium transport through a single molecule transistor is investigated by using the improved canonical transformation scheme and extended equation of motion approach. Two types of Kondo phonon-satellite with different asymmetric shapes are fully confirmed in the spectral function, and are related to the electron spin singlet or hole spin singlet, respectively. Moreover, when a moderate Zeeman splitting is caused by a local magnetic field, the Kondo satellites in the spin-resolved spectral function are found to disappear on one side of the main peak, and they disappear on the opposite side for the opposite spin component. All these peculiar signatures that manifest themselves in the nonlinear differential conductance are explained with a clear physics picture.

(Some figures in this article are in colour only in the electronic version)

1. Introduction

The Kondo effect as a manifestation of strong correlations between conduction electrons and spin impurity has been extensively studied in the context of quantum dot physics in past years [1–7]. Recently, its realization in the single-molecule transistor (SMT) has attracted a lot of attention [8–14]. In particular, the latest experiments in an SMT, in which the phonon-satellite has been clearly observed even in the Kondo regime [15–17] owing to the enhanced electron–vibration coupling in the molecule [18–20], has stimulated great interest to investigate the interplay of the electron–phonon interaction (EPI) and the Kondo effect in the transport through the SMT.

According to our recent investigation on the spectral function of the SMT in the absence of Coulomb interaction, the phonon-satellites are quite sensitive to the lead Fermi levels with respect to the localized level [21]. When the temperature is too low to excite phonons thermally,

the phonon-satellites can only develop below (above) the resonant level if this level is occupied (empty) initially, as then electrons can only emit phonons. On the other hand, in the Kondo regime with the EPI ignored, it is well known that two collective spin singlet states will be formed between the localized state and the excited electron states above the Fermi level μ or the excited hole states below μ because of spin exchange processes [22, 23], which will contribute to the formation of the sharp Kondo peak pinning at the Fermi surface in the local density of states. It is thus expected that interesting transport physics may result from the interplay of both the EPI and the Kondo effect, in particular out of the equilibrium, as both effects are sensitive to the Fermi levels at the source and drain electrode.

Several theoretical techniques have been developed and applied to address the joint effects of the EPI and the Kondo correlation on transport through a quantum dot or an SMT [24–34]. According to these works, the equilibrium properties, in particular the renormalized effect on the Kondo correlation due to the EPI, have been well described. For example, with the help of the numerical renormalization group approach, the renormalized effect has been predicted for a wide range of parameters in the equilibrium [26–29]. With the help of a generalized Schrieffer–Wolff transformation, under the assumption that the system stays in equilibrium in the strongly asymmetric coupling case, the nonlinear differential conductance has been given [30] with the Kondo satellite structure exhibited. On the other hand, owing to the lack of satisfactory treatment for the nonequilibrium Kondo problem, little effort has been made to investigate how the Kondo phonon-satellites develop and manifest themselves in the nonequilibrium transport. However, since the Kondo phonon-satellites can only be observed at finite bias voltage experimentally, when the system is driven out of equilibrium [15–17], it is certainly of importance to investigate the key signature of the nonequilibrium Kondo phonon effect. As far as we know, by the real-time diagrammatic formulation, Köning *et al* have given the spectral function as well as the differential conductance with Kondo satellites in the nonequilibrium situation [24, 25]. Here we shall develop another easier and straightforward approach, which will combine the improved non-perturbative canonical transformation treatment of the EPI [21] with the extended equation-of-motion (EOM) method of the nonequilibrium Green functions. This approach, although it is not rigorous in quantitative description, has the advantage of intuitiveness and can provide a semi-quantitative understanding of the phonon-assisted Kondo effect, particularly for strong electron–vibration coupling, as well as for the nonequilibrium situation.

Based on the approach mentioned above, in the present paper, we shall mainly focus on how the Kondo satellites develop and manifest themselves in the nonequilibrium transport through the SMT, and how these Kondo satellites are affected by an applied local magnetic field. Following this introduction, we shall give our model and method in section 2 and 3, respectively. Our main results are presented in section 4, which include: (i) the Kondo phonon-satellites may exhibit quite different asymmetric line-shapes with respect to the Kondo main peak in the spectral function, and also in the nonlinear differential conductance; (ii) two types of spin exchange processes, associated with the collective spin singlets formed by electron states and by hole states respectively, can be clearly distinguished by the Kondo satellites; and (iii) with a moderate Zeeman splitting exceeding the width of Kondo peak, its Kondo phonon-satellites only appear on one side of the main Kondo peak in one spin-resolved spectral function, and on the opposite side for the opposite spin component. Finally, the conclusions are drawn.

2. Model

The SMT system studied in the present paper can usually be described as the Anderson–Holstein model, in which a single localized state coupled linearly to one local vibration mode

and to the left (L) and right (R) non-interacting leads, namely

$$\mathbf{H} = \sum_{\alpha;\mathbf{k},\sigma} \varepsilon_{\alpha\mathbf{k}} \mathbf{c}^{\dagger}_{\alpha\mathbf{k}\sigma} \mathbf{c}_{\alpha\mathbf{k}\sigma} + \sum_{\sigma} \varepsilon_{\sigma} \mathbf{n}_{\sigma} + U_0 \mathbf{n}_{\uparrow} \mathbf{n}_{\downarrow} + \hbar\omega_0 \mathbf{a}^{\dagger}\mathbf{a} + \sum_{\sigma} \lambda \mathbf{n}_{\sigma} (\mathbf{a}^{\dagger} + \mathbf{a}) + \sum_{\alpha;\mathbf{k},\sigma} (V_{\alpha\mathbf{k}} \mathbf{c}^{\dagger}_{\alpha\mathbf{k}\sigma} \mathbf{d}_{\sigma} + \text{h.c.}), \tag{1}$$

where $\mathbf{c}^{\dagger}_{\alpha\mathbf{k}\sigma}$ ($\mathbf{c}_{\alpha\mathbf{k}\sigma}$) and $\mathbf{d}^{\dagger}_{\sigma}$ ($\mathbf{d}_{\sigma}$) are the creation (annihilation) operators for the lead electron with energy $\varepsilon_{\alpha\mathbf{k}}$ and the localized SMT electron with energy ε_{σ}, respectively, σ denotes the spin index and the lead index $\alpha = \mathrm{L}, \mathrm{R}$. U_0 is the on-site Coulomb repulsion, and $\mathbf{n}_{\sigma} = \mathbf{d}^{\dagger}_{\sigma}\mathbf{d}_{\sigma}$. The operator $\mathbf{a}^{\dagger}$ ($\mathbf{a}$) creates (annihilates) the local vibration mode with frequency ω_0, λ is the EPI strength, and $V_{\alpha\mathbf{k}}$ is the tunnelling coupling between the localized and lead electrons, which results in a level broadening $\Gamma = (\Gamma_{\mathrm{L}} + \Gamma_{\mathrm{R}})/2$, where

$$\Gamma_{\alpha}(\omega) \equiv 2\pi \sum_{\mathbf{k}} |V_{\alpha\mathbf{k}}|^2 \delta(\omega - \varepsilon_{\alpha\mathbf{k}}). \tag{2}$$

To treat the EPI non-perturbatively, by the canonical transformation, $\mathbf{S} = \frac{\lambda}{\omega_0} \sum_{\sigma} \mathbf{n}_{\sigma} (\mathbf{a}^{\dagger} - \mathbf{a})$, the Hamiltonian is transformed into $\bar{\mathbf{H}} \equiv e^{\mathbf{S}} \mathbf{H} e^{-\mathbf{S}} = \bar{\mathbf{H}}_{\mathrm{ph}} + \bar{\mathbf{H}}_{\mathrm{el}}$, where the phonon part $\bar{\mathbf{H}}_{\mathrm{ph}} = \hbar\omega_0 \mathbf{a}^{\dagger}\mathbf{a}$, and the electron part turns out to be the Anderson Hamiltonian, namely

$$\bar{\mathbf{H}}_{\mathrm{el}} = \sum_{\alpha,\mathbf{k},\sigma} \varepsilon_{\alpha\mathbf{k}} \mathbf{c}^{\dagger}_{\alpha\mathbf{k}\sigma} \mathbf{c}_{\alpha\mathbf{k}\sigma} + \sum_{\sigma} \bar{\varepsilon}_{\sigma} \mathbf{n}_{\sigma} + \bar{U}_0 \mathbf{n}_{\uparrow} \mathbf{n}_{\downarrow} + \sum_{\alpha,\mathbf{k},\sigma} (\bar{V}_{\alpha\mathbf{k}} \mathbf{c}^{\dagger}_{\alpha\mathbf{k}\sigma} \mathbf{d}_{\sigma} + \text{h.c.}). \tag{3}$$

The parameters with a bar in equation (3) correspond to the renormalized ones resulting from the canonical transformation, i.e., the SMT level is shifted to $\bar{\varepsilon}_{\sigma} = \varepsilon_{\sigma} - g\omega_0$ with $g \equiv (\lambda/\omega_0)^2$, and the on-site repulsion is renormalized to $\bar{U}_0 = U_0 - 2g\omega_0$. When the charging energy is significantly reduced by screening due to the electrodes [35], $\bar{U}_0$ may become negative for very strong EPI, which will result in the anisotropic Kondo effect [26–29]. But in most realistic situations, the charging energy is much larger than the EPI energy [18–20], so we shall limit ourselves to the standard Kondo effect, i.e. $\bar{U}_0$ remains positive. Besides, $\bar{V}_{\sigma\mathbf{k}} \equiv V_{\sigma\mathbf{k}}\mathbf{X}$ with $\mathbf{X} \equiv \exp[-(\lambda/\omega_0)(\mathbf{a}^{\dagger} - \mathbf{a})]$, indicating that a cloud of phonons will be created or destroyed during the hopping processes. As it contains the phonon operator $\mathbf{X}$, the renormalized Hamiltonian $\bar{\mathbf{H}}_{\mathrm{el}}$ has not been fully decoupled. For the present work, we are specially interested in the cases where the EPI is sufficiently strong compared to the tunnelling coupling so that a local polaron is formed. Then we can approximate the phonon operator $\mathbf{X}$ by its expectation value in the thermal equilibrium, $\langle \mathbf{X} \rangle = \exp[-g(N_{\mathrm{ph}} + 1/2)]$, with N_{ph} defined as the population of phonons at temperature T. Although it uses the mean field approximation, this method has been used widely and has obtained reasonable successes [36–41].

With this mean field approximation, the lesser Green function can then be separated into the electron part and phonon part,

$$G^{<}_{\sigma}(t) \equiv \mathrm{i} \langle \mathbf{d}^{\dagger}_{\sigma}(0) \mathbf{d}_{\sigma}(t) \rangle = \mathrm{i} \left\langle \overline{\mathbf{d}}^{\dagger}_{\sigma} \mathrm{e}^{\mathrm{i}\overline{\mathbf{H}}t} \overline{\mathbf{d}}_{\sigma} \mathrm{e}^{-\mathrm{i}\overline{\mathbf{H}}t} \right\rangle = \mathrm{i} \left\langle \mathbf{d}^{\dagger}_{\sigma} \mathrm{e}^{\mathrm{i}\overline{\mathbf{H}}_{\mathrm{el}}t} \mathbf{d}_{\sigma} \mathrm{e}^{-\mathrm{i}\overline{\mathbf{H}}_{\mathrm{el}}t} \right\rangle_{\mathrm{el}} \left\langle \mathbf{X}^{\dagger} \mathrm{e}^{\mathrm{i}\overline{\mathbf{H}}_{\mathrm{ph}}t} \mathbf{X} \mathrm{e}^{-\mathrm{i}\overline{\mathbf{H}}_{\mathrm{ph}}t} \right\rangle_{\mathrm{ph}}. \tag{4}$$

The trace of the phonon part can be evaluated by the Feynman disentangling technique [39]. The lesser Green function of the SMT electron can be decoupled as

$$G^{<}_{\sigma}(\omega) = \sum_{n=-\infty}^{\infty} L_n \bar{G}^{<}_{\sigma}(\omega + n\omega_0), \tag{5}$$

and similarly the greater Green function is formulated as

$$G^{>}_{\sigma}(\omega) = \sum_{n=-\infty}^{\infty} L_n \bar{G}^{>}_{\sigma}(\omega - n\omega_0). \tag{6}$$

Here $\bar{G}_\sigma^{>(<)}$ is the dressed Green function associated with $\bar{\mathbf{H}}_{\rm el}$, and

$$L_n = \mathrm{e}^{-g\left(2N_{\rm ph}+1\right)}\mathrm{e}^{n\omega_0/2k_{\rm B}T}\, I_n\left(2g\sqrt{N_{\rm ph}\left(N_{\rm ph}+1\right)}\right), \tag{7}$$

in which $I_n(z)$ is the nth Bessel function of the complex argument. The spectral function is then calculated with the lesser and greater Green functions via

$$A_\sigma(\omega) = \mathrm{i}(G_\sigma^{>}(\omega) - G_\sigma^{<}(\omega)). \tag{8}$$

It should be emphasized that people usually evaluate the spectral function via $A_\sigma(\omega) = \mathrm{i}(G_\sigma^{\rm r}(\omega) - G_\sigma^{\rm a}(\omega))$, in which the retarded and advanced Green functions, $G_\sigma^{\rm r}$ and $G_\sigma^{\rm a}$, are approximately separated into the electron and phonon parts by ignoring the difference between $N_{\rm ph}$ and $N_{\rm ph}+1$, which works only in the high-temperature limit [36–38]. However, the Kondo phonon problem studied here is certainly not the case, as the characteristic Kondo temperature, $T_{\rm K}$, is very low. Hence the prescription we have recently made may be more appropriate [21].

3. Keldysh Green functions

Within the Keldysh formalism, the dressed Green functions $\bar{G}_\sigma^{>(<)}$ can be derived from $\bar{\mathbf{H}}_{\rm el}$ with the help of the EOM approach. Since the usual approximation in decoupling the higher-order Green functions generated by the EOM is valid only near or above the Kondo temperature $T_{\rm K}$ [42, 43], at lower temperature, as in the present situation, the approximation developed by Lacroix may be more appropriate [44]. In the original Lacroix approach, only a system with spin degeneracy and infinite charging energy was discussed in the equilibrium. To apply to the nonequilibrium situation with finite U_0 and Zeeman splitting, we have extended it accordingly. Thus, the usually ignored higher-order retarded Green functions are taken into reconsideration. For example, $\langle\langle \mathbf{d}_{\bar\sigma}\mathbf{c}^\dagger_{\alpha\mathbf{k}\bar\sigma}\mathbf{c}_{\alpha'\mathbf{k}'\sigma}, \mathbf{d}^\dagger_\sigma\rangle\rangle$ is now approximately decoupled as $\langle \mathbf{d}_{\bar\sigma}\mathbf{c}^\dagger_{\alpha\mathbf{k}\bar\sigma}\rangle\langle\langle \mathbf{c}_{\alpha'\mathbf{k}'\sigma}, \mathbf{d}^\dagger_\sigma\rangle\rangle$, and the matrix element $\langle \mathbf{d}_{\bar\sigma}\mathbf{c}^\dagger_{\alpha\mathbf{k}\bar\sigma}\rangle$ should be determined self-consistently by the nonequilibrium Green function technique.

From the standard derivation of the EOM [45][3], the dressed retarded Green function turns out to be

$$\begin{aligned}\bar{G}_\sigma^{\rm r}(\omega) = {} & \frac{1-\left(\langle\bar{\mathbf{n}}_{\bar\sigma}\rangle + \bar{P}_{\bar\sigma}(\bar\omega^0_{\bar\sigma}) + \bar{P}^*_{\bar\sigma}(-\bar\omega^U)\right)}{\omega-\bar\varepsilon_\sigma - \bar\Sigma^{(T)}(\omega) + \frac{\bar{U}_0\bar\Sigma^{(1)}_{\bar\sigma}(\omega)}{\omega-\bar\varepsilon_\sigma-\bar{U}_0-\bar\Sigma^{(T)}(\omega)-\bar\Sigma^{(3)}_{\bar\sigma}(\omega)}} \\ & + \frac{\langle\bar{\mathbf{n}}_{\bar\sigma}\rangle + \bar{P}_{\bar\sigma}(\bar\omega^0_{\bar\sigma}) + \bar{P}^*_{\bar\sigma}(-\bar\omega^U)}{\omega-\bar\varepsilon_\sigma-\bar{U}_0-\bar\Sigma^{(T)}(\omega) - \frac{\bar{U}_0\bar\Sigma^{(2)}_{\bar\sigma}(\omega)}{\omega-\bar\varepsilon_\sigma-\bar\Sigma^{(T)}(\omega)-\bar\Sigma^{(3)}_{\bar\sigma}(\omega)}},\end{aligned} \tag{9}$$

where

$$\begin{aligned}\bar\omega^0_{\bar\sigma} &\equiv \omega + \bar\varepsilon_{\bar\sigma} - \bar\varepsilon_\sigma, \\ \bar\omega^U &\equiv \omega - \bar\varepsilon_\sigma - \bar\varepsilon_{\bar\sigma} - \bar{U}_0,\end{aligned} \tag{10}$$

and the correlation function between the SMT level and leads, $\bar{P}_{\bar\sigma}(\omega)$, is defined as

$$\bar{P}_{\bar\sigma}(\omega) \equiv \sum_{\alpha\mathbf{k}} \bar{V}^*_{\alpha\mathbf{k}}\langle \mathbf{d}^\dagger_{\bar\sigma}\mathbf{c}_{\alpha\mathbf{k}\bar\sigma}\rangle g^{\rm r}_{\alpha\mathbf{k}}(\omega), \tag{11}$$

[3] After submitting our manuscript, a closely related work by V Kashcheyevs *et al* with similar (with a slightly different truncated approximation) EOM derivations of the Green functions has appeared; the details of the derivation can be found in their appendix [46].

in which $g^{\rm r}_{\alpha\mathbf{k}}(\omega)$ is the unperturbed retarded Green function of the lead electron. In the above the self-energy associated with the resonant tunnelling processes is defined as

$$\bar{\Sigma}^{(T)}(\omega) \equiv \sum_{\alpha\mathbf{k}} |\bar{V}_{\alpha\mathbf{k}}|^2 g^{\rm r}_{\alpha\mathbf{k}}(\omega), \tag{12}$$

and the self-energies related to the Kondo correlation are respectively expressed as

$$\begin{aligned}
\bar{\Sigma}^{(1)}_{\bar{\sigma}}(\omega) &= \bar{\Sigma}^{(0)}_{\bar{\sigma}}(\omega) - \bar{\Sigma}^{(T)}(\omega)\left[\bar{P}_{\bar{\sigma}}(\bar{\omega}^0_\sigma) + \bar{P}^*_{\bar{\sigma}}(-\bar{\omega}^U)\right], \\
\bar{\Sigma}^{(3)}_{\bar{\sigma}}(\omega) &= \bar{\Sigma}^{(T)}(\bar{\omega}^0_{\bar{\sigma}}) - \left(\bar{\Sigma}^{(T)}(-\bar{\omega}^U)\right)^*, \\
\bar{\Sigma}^{(2)}_{\bar{\sigma}}(\omega) &= \bar{\Sigma}^{(3)}_{\bar{\sigma}}(\omega) - \bar{\Sigma}^{(1)}_{\bar{\sigma}}(\omega).
\end{aligned} \tag{13}$$

Here $\bar{\Sigma}^{(0)}_{\bar{\sigma}}(\omega) = \bar{F}_{\bar{\sigma}}(\bar{\omega}^0_{\bar{\sigma}}) - \bar{F}^*_{\bar{\sigma}}(-\bar{\omega}^U) + \bar{B}_{\bar{\sigma}}(\omega)$,

$$\bar{F}_{\bar{\sigma}}(\omega) = \sum_{\alpha\mathbf{k},\alpha'\mathbf{k}'} \bar{V}^*_{\alpha\mathbf{k}} \bar{V}_{\alpha'\mathbf{k}'} \langle \mathbf{c}^\dagger_{\alpha'\mathbf{k}'\bar{\sigma}} \mathbf{c}_{\alpha\mathbf{k}\bar{\sigma}} \rangle g^{\rm r}_{\alpha\mathbf{k}}(\omega), \tag{14}$$

and

$$\bar{B}_{\bar{\sigma}}(\omega) = -2{\rm i}\,{\rm Im}\left\{\sum_{\alpha'\mathbf{k}'} \bar{V}^*_{\alpha'\mathbf{k}'} \left\langle \mathbf{d}^\dagger_{\bar{\sigma}} \mathbf{c}_{\alpha'\mathbf{k}'\bar{\sigma}} \right\rangle\right\}\left[\sum_{\alpha\mathbf{k}} |\bar{V}_{\alpha\mathbf{k}}|^2 \left(g^{\rm r}_{\alpha\mathbf{k}}(\omega)\right)^2\right]. \tag{15}$$

In the wide-band limit, $\bar{\Sigma}^{(T)}(\omega) \approx -{\rm i}\bar{\Gamma}$, and

$$\bar{\Sigma}^{(0)}_{\bar{\sigma}}(\omega) \approx \sum_\alpha \frac{\bar{\Gamma}_\alpha}{2\pi}\left[\psi\left(\frac{1}{2} + \frac{\bar{\omega}^U + \mu_\alpha}{{\rm i}2\pi k_{\rm B}T}\right) - \psi\left(\frac{1}{2} + \frac{\bar{\omega}^0_{\bar{\sigma}} - \mu_\alpha}{{\rm i}2\pi k_{\rm B}T}\right) - {\rm i}\pi\right], \tag{16}$$

where the Psi function ψ is the logarithmic derivative of the gamma function. Now the self-consistent equation for $\bar{P}_{\bar{\sigma}}(\omega)$ is simplified as

$$\bar{P}_{\bar{\sigma}}(\omega) = \int \frac{{\rm d}\,\omega'}{2\pi} \frac{[\bar{\Gamma}_{\rm L} f_{\rm L}(\omega') + \bar{\Gamma}_{\rm R} f_{\rm R}(\omega')]\bar{G}^{r*}_{\bar{\sigma}}(\omega')}{\omega - \omega' + {\rm i}0^+}, \tag{17}$$

which, together with equation (9), gives the dressed retarded Green function $\bar{G}^{\rm r}_\sigma$.

As we will see, at zero temperature, not only $\bar{F}_{\bar{\sigma}}(\omega)$, but also $\bar{P}_{\bar{\sigma}}(\omega)$ will diverge logarithmically and then both contribute to the sharp Kondo resonance at each Fermi surface. Therefore, $\bar{P}_{\bar{\sigma}}(\omega)$ should not be ignored as in the previous approaches [42, 43]. Generally, this EOM approach works for most cases; however, it fails to give the Kondo resonance in the particle–hole symmetric case. For example, when $\bar{\varepsilon}_\uparrow = \bar{\varepsilon}_\downarrow = -\bar{U}_0/2$, equations (10), (11), (14) show that $\bar{\omega}^0_\sigma = \bar{\omega}^U$, $\bar{P}^*_{\bar{\sigma}}(-\omega) = -\bar{P}_{\bar{\sigma}}(\omega)$, and $\bar{F}^*_{\bar{\sigma}}(-\omega) = -\bar{F}_{\bar{\sigma}}(\omega)$. Therefore the divergent terms in the expression of the retarded Green function are cancelled with each other and then no Kondo resonance will show up[4]. The reason for this limitation is the fact that at the particle–hole symmetry point, the charge fluctuations are completely quenched; therefore the EOM approach cannot be applied [14].

By the Keldysh formula $\bar{G}^{>(<)}_\sigma = \bar{G}^{\rm r}_\sigma \bar{\Sigma}^{>(<)}_\sigma \bar{G}^{\rm a}_\sigma$, in which the greater (lesser) self-energy is evaluated by the ansatz adopted by Ng [47], the dressed greater and lesser Green functions are obtained as

$$\begin{aligned}
\bar{G}^{>}_\sigma(\omega) &= {\rm i}([\bar{\Gamma}_{\rm L}(1 - f_{\rm L}(\omega)) + \bar{\Gamma}_{\rm R}(1 - f_{\rm R}(\omega))])\,{\rm Im}\,\bar{G}^{\rm r}_\sigma(\omega)/\bar{\Gamma}, \\
\bar{G}^{<}_\sigma(\omega) &= -{\rm i}[\bar{\Gamma}_{\rm L} f_{\rm L}(\omega) + \bar{\Gamma}_{\rm R} f_{\rm R}(\omega)]\,{\rm Im}\,\bar{G}^{\rm r}_\sigma(\omega)/\bar{\Gamma}.
\end{aligned} \tag{18}$$

Substituting equation (18) into equations (5) and (6), one obtains the greater (lesser) Green function and subsequently the spectral function of the SMT.

It is noted that, with the infinity charging energy and zero Zeeman splitting in the equilibrium, our results will recover to Lacroix's one [44]. Together with the

[4] The drawback of the EOM at the particle–hole symmetric point has also been discussed in [46].

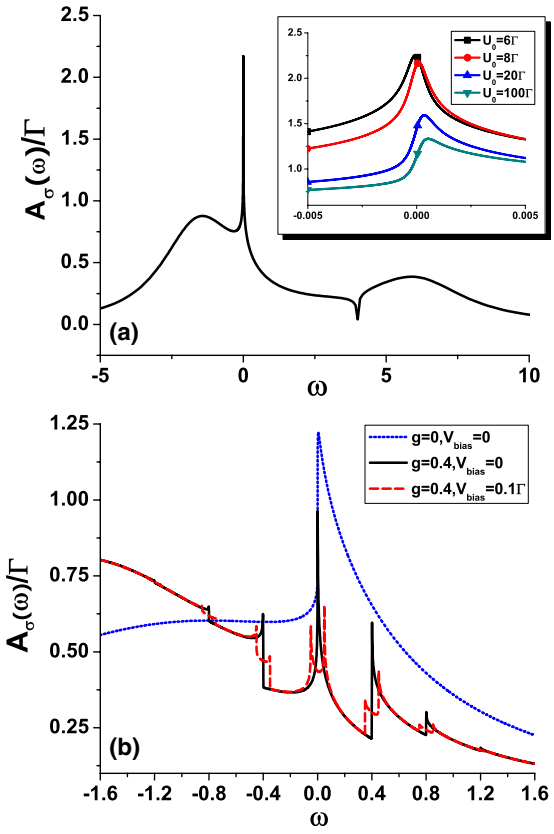

Figure 1. The spectral functions of the spin-degenerate local electrons, i.e., A_σ, with (a) and without (b) the EPI. The parameters used in (a) are $\mu_L = \mu_R = 0.0$, $\varepsilon_0 = -2\Gamma$, and $U_0 = 8\Gamma$, $V_{bias} = 0$. The parameters used in (b) are $(\mu_L + \mu_R)/2 = 0$, $\varepsilon_0 = -2.5\Gamma$, $k_B T = 2 \times 10^{-4}\Gamma$, $U_0 = 100\Gamma$, $\hbar\omega_0 = 0.4\Gamma$. Other parameters have been shown explicitly in each figure.

improved canonical transformation, this generalized EOM method will be our framework for investigating the Kondo satellites at the nonequilibrium with finite Zeeman splitting. Although this approach can only give a qualitative description of the shape of the Kondo satellites, it does predict the correct peak positions [26, 42, 43]. For quantitative description of the renormalized properties in the equilibrium or exploring wider parameter space, more accurate methods like the numerical renormalization group (NRG) approach or quantum Monte Carlo calculations may be appropriate [26–29].

With the spectral function and the lesser Green function given above, the current through the SMT can be calculated via [48, 49]

$$J = \sum_\sigma \frac{ie}{2h} \int d\omega \{[f_L(\omega)\Gamma_L - f_R(\omega)\Gamma_R]A_\sigma(\omega) + (\Gamma_L - \Gamma_R)G^<_\sigma(\omega)\}, \tag{19}$$

and the differential conductance can be obtained straightforwardly as $G = \partial J/\partial V_{bias}$.

4. Spectral function and differential conductance

4.1. Spin-degenerate case

First, we will discuss the spin-degenerate case, i.e., $\varepsilon_\uparrow = \varepsilon_\downarrow = \varepsilon_0$. The spectral function in the absence of the EPI is plotted in figure 1(a) for different U_0, which shows that besides the two

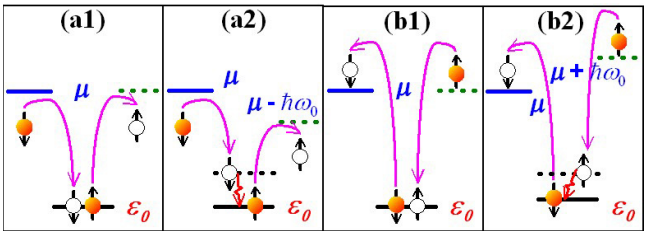

Figure 2. Schematic illustration for the spin exchange processes associated with the formation of the Kondo satellites.

broad resonant peaks at $\bar{\varepsilon}_0$ and $\bar{\varepsilon}_0 + \bar{U}_0$, there will be a sharp Kondo resonance developed at $\mu_{\mathrm{L(R)}}$. By increasing $\bar{U}_0$, as can be observed from the inset of figure 1(a), this Kondo resonant peak can be tuned to be more and more asymmetric, which is a manifestation of the particle–hole asymmetry of the SMT.

When the electron–phonon interaction is turned on, as shown in figure 1(b), the Kondo peak will be split into a set of phonon-satellites spaced by a multiple of the phonon frequency. When the system is driven out of equilibrium by applying a bias voltage, the main Kondo peak will be split into two weakened peaks pinned at the Fermi levels of the left and right lead, respectively, and the Kondo phonon-satellites will also be split into two corresponding sub-sets. These results agree well with previous works, which validates the present framework [24, 25, 42, 43].

The underlying physics about how and why the Kondo satellites develop in such a way can be intuitively understood with the help of figure 2. As illustrated by figure 2(a1), a local hole state in the SMT exchanges with the excited holes at leads below the Fermi energy μ to form a Kondo spin-singlet. When an electron hops to the local state by emitting a phonon, as shown in figure 2(a2), only the holes with energy below $\mu - \hbar\omega_0$ can exchange with the local hole, because the phonon absorption is unavailable at very low temperature and the energy conservation law must be satisfied in the interaction process. Thus a phonon-satellite peak at $\mu - \hbar\omega_0$ appears in the density of states or tunnelling spectra. Similarly, a spin-singlet consisting of a localized electron and excited electrons above μ is depicted in figure 2(b1), and only the electrons above $\mu + \hbar\omega_0$ can exchange with the local electron if the hopping processes are accompanied by emitting a phonon as shown in figure 2(b2), which will give rise to the satellite peak at $\mu + \hbar\omega_0$. That means although both processes shown in figures 2(a1) and (b1) contribute to the main Kondo peak, they can be distinguished by their Kondo satellites, namely, the contributions of each type of exchange processes to the Kondo peak can be picked out in principle by comparing with the satellites on each side of the main peak.

Figure 1(b) also shows that the satellites on different sides of the Kondo main peak may take on apparent sharp asymmetric lineshapes. The reason for these sharp feature lies in the sharp Fermi distributions in the leads at very low temperature, where the electron excitations and the hole excitations are separated from each other sharply by the Fermi surface. For example, the phonon-assisted spin exchange processes mentioned above have sharp energy boundaries as $\mu_{\mathrm{L(R)}} \pm n\omega_0$; therefore they may result in the sharp features at $\omega = \mu_{\mathrm{L(R)}} \pm n\omega_0$ as shown in figure 1(b). Besides, if the localized level is broadened so that there is a finite density of states around $\mu_{\mathrm{L(R)}}$, the electron can also bypass the SMT via the phonon-assisted resonant tunnelling processes. According to our previous studies [21], these phonon-assisted resonant tunnelling processes can result in the phonon sidebands at $\omega = \bar{\varepsilon}_0 \pm n\omega_0$, which also exhibit some sharp asymmetric lineshapes at $\omega = \mu_{\mathrm{L(R)}} \pm n\omega_0$ under extremely low temperature.

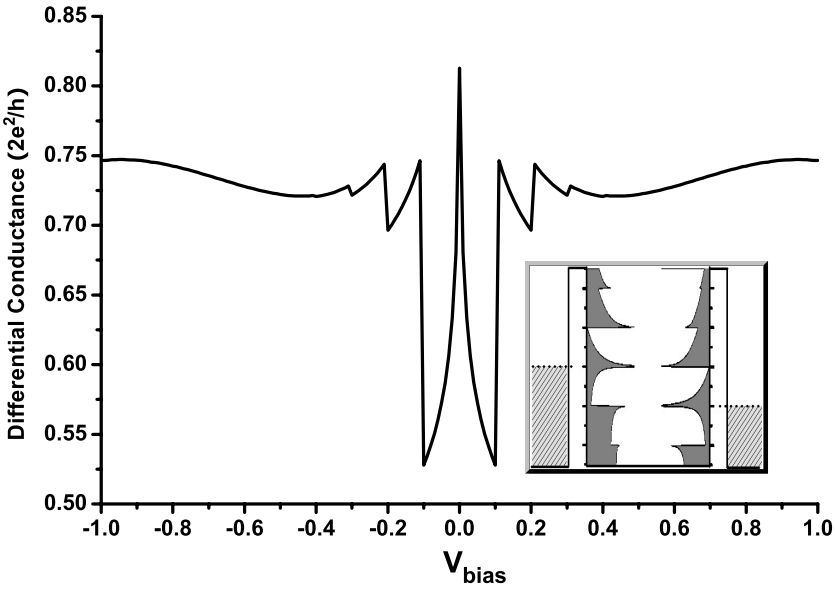

Figure 3. The differential conductance for the spin-degenerate case as a function of the bias voltage. Here $\tilde{\epsilon}_0 = -2.5\Gamma$, $g = 0.5$, $k_B T = 2 \times 10^{-4}\Gamma$, $U_0 = 100\Gamma$, and $\hbar\omega_0 = 0.1\Gamma$. As an illustration, the inset shows the origin of the first Kondo phonon-satellite peak schematically.

These structures superpose over the Kondo phonon-satellites, being jointly responsible for the apparent sharp asymmetric peaks observed in figure 1(b).

The nonlinear differential conductance versus the bias voltage, i.e., $G(V_{\rm bias})$, is plotted in figure 3 for very low temperature, where G reaches a peak value at $V_{\rm bias} = 0$ and then decreases rapidly as $V_{\rm bias}$ increases. This zero-bias anomaly is usually regarded as the experimental evidence for the Kondo effect in quantum dot systems. When $eV_{\rm bias} = n\hbar\omega_0$, there are some Kondo phonon-satellite peaks that show up, as evidenced by very recent experiments [15–17]. According to the general understanding, in the non-EPI case the bias voltage plays a role similar to temperature, which means that the differential conductance decreases logarithmically as $V_{\rm bias}$ increases [50]. One may wonder here why the apparent sharp asymmetric features of the Kondo phonon peaks in figure 3 have not been smoothed out by bias voltage. It is because the Fermi distributions in the leads have sharp Fermi surfaces at very low temperature; hence the sharp features of the spectral function, as shown in figure 1(b), can still be preserved even for finite bias voltage. As illustrated in the inset of figure 3, once an asymmetric peak in the spectral function matches one of the Fermi levels, a sharp asymmetric differential conductance peak will appear. Therefore, the apparent sharp asymmetric features in $G(V_{\rm bias})$ are just the manifestations of the asymmetric lineshapes of the spectral function, which contain both contributions from the phonon-assisted Kondo processes and the phonon-assisted resonant tunnelling processes as well. These sharp asymmetric features can only be smoothed out with the increasing temperature.

It is worth pointing out the resemblances between our spin-degenerate results and those by the real-time diagrammatic formulation [24, 25] or the generalized Schrieffer–Wolff transformation [30], where the discontiguous and asymmetric lineshape features of the Kondo phonon-satellites in the spectral function or the differential conductance can also be observed, but have not yet been clearly pointed out and properly explained.

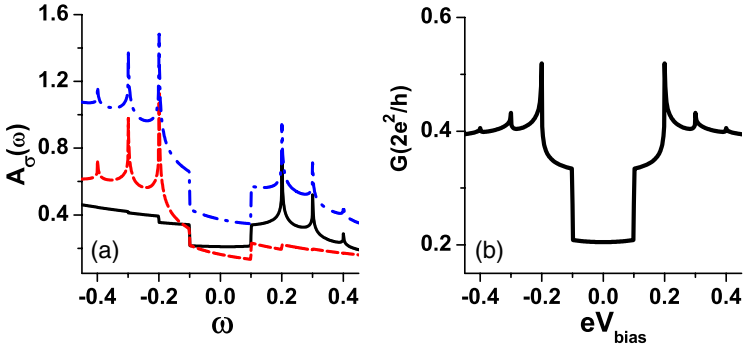

Figure 4. The calculated total (dash–dotted (blue)) and spin-resolved (solid (black) line for spin-up, and dashed (red) line for spin-down) spectral functions in the equilibrium (a), and the nonlinear differential conductance (b) in the presence of finite Zeeman splitting. Here $\bar{\varepsilon}_0 = -2.5\Gamma$, $g = 0.6$, $k_B T = 2 \times 10^{-4}\Gamma$, $U_0 = 100\Gamma$, $\hbar\omega_0 = 0.1\Gamma$, and $\Delta = 0.2\Gamma$.

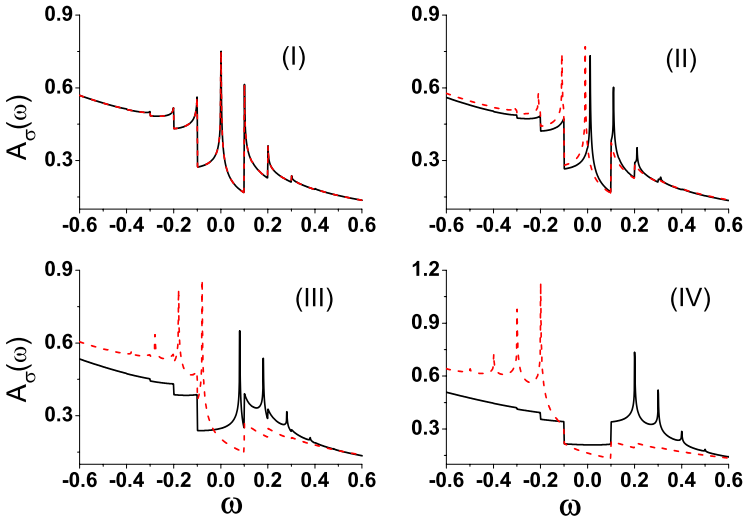

Figure 5. The spin-resolved spectral function (solid (black) line for spin-up, dashed (red) line for spin-down component) for different Zeeman splitting: (I) $\Delta = 0$, (II) $\Delta = 0.01\Gamma$, (III) $\Delta = 0.08\Gamma$, and (IV) $\Delta = 0.2\Gamma$. The other parameters are taken as $V_{bias} = 0$, $\bar{\varepsilon}_0 = -2.5\Gamma$, $g = 0.6$, $U_0 = 100\Gamma$, and $\hbar\omega_0 = 0.1\Gamma$.

4.2. Finite Zeeman splitting case

Now let us take a look at the spin non-degenerate case, where a Zeeman splitting of Δ for the localized level may be induced by a local magnetic field, i.e. $\varepsilon_\uparrow = \varepsilon_0 + \Delta/2$ and $\varepsilon_\downarrow = \varepsilon_0 - \Delta/2$.

Without the EPI, our calculation for the spin-splitting case shows that, compared to the spin-degenerate case, the Kondo peak in the spin-resolved spectral function $A_\uparrow(\omega)$ (or $A_\downarrow(\omega)$) generally decreases in magnitude and shifts away from μ by Δ $(-\Delta)$, which agrees with previous researches [24–29, 42, 43]. When the EPI turns on, as shown in figure 4(a), the phonon-satellite structure may develop in a distinct way, that is, for moderate Zeeman splitting only the satellites above (below) the main peak appear in $A_\uparrow(\omega)$ ($A_\downarrow(\omega)$).

This peculiar feature in the spin-resolved spectral function stems from the interplay between the EPI and Kondo effect in the presence of the finite spin-splitting. It also manifests

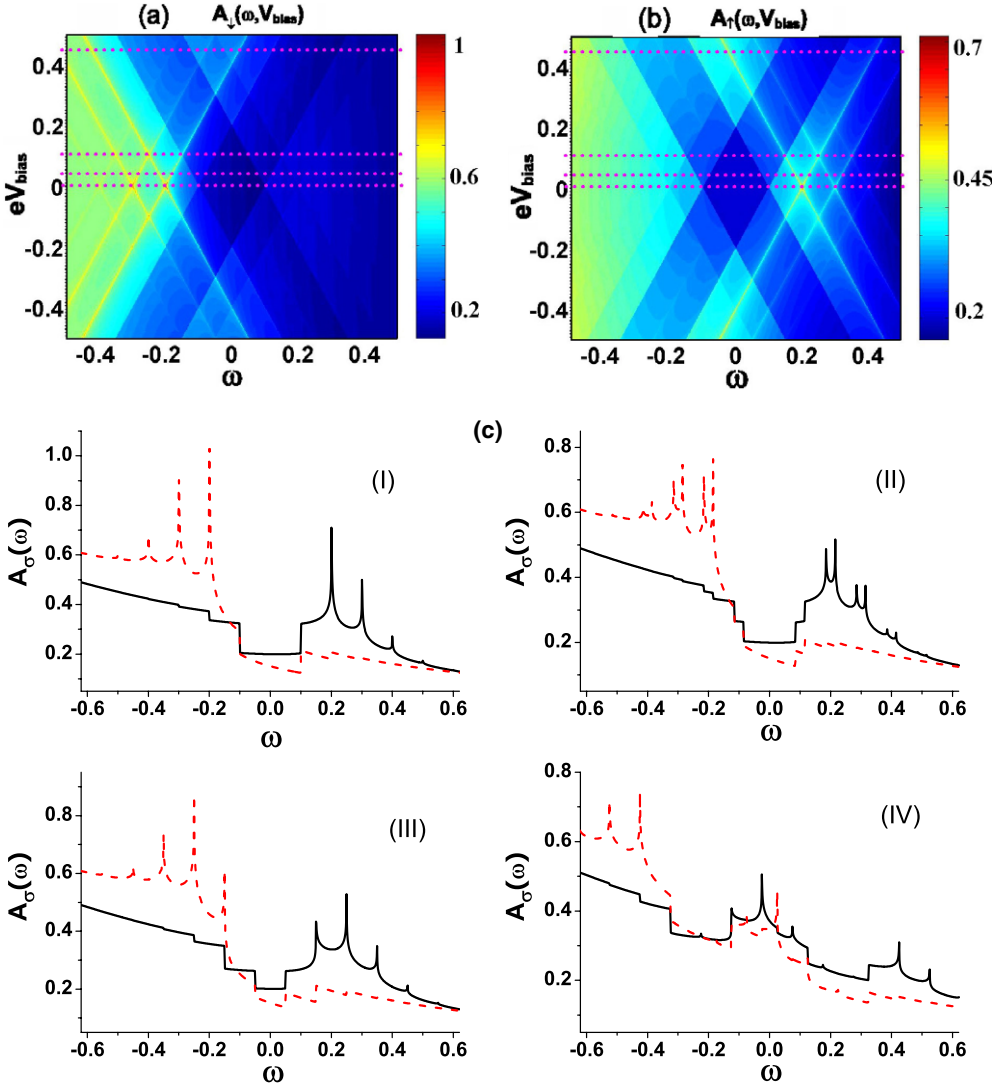

Figure 6. Maps for the spin-up (a) and spin-down (b) spectral functions as functions of ω and $eV_{\rm bias}$. The sections are plotted in (c) for four typical bias voltages: (I) $eV_{\rm bias} = 0$, (II) $eV_{\rm bias} = 0.03\Gamma$, (III) $eV_{\rm bias} = 0.1\Gamma$, (IV) $eV_{\rm bias} = 0.45\Gamma$. Here $\Delta = 0.2\Gamma$, $\tilde{\varepsilon}_0 = -2.5\Gamma$, $g = 0.6$, $U_0 = 100\Gamma$, and $\hbar\omega_0 = 0.1\Gamma$.

itself in the differential conductance. As shown in figure 4(b), there is no satellite appearing in the region $\mu - \Delta < eV_{\rm bias} < \mu + \Delta$, which is generally true as long as the system is at very low temperature. According to our simple picture above (cf figure 2), this is easy to understand.

The spin-resolved spectral functions for four different Zeeman splitting values are plotted in figure 5, demonstrating that when the Zeeman splitting turns on, the overall Kondo peaks in the spin-down spectral function shift towards the low energy, while those for spin-up undergo a blue shift. The Kondo satellites above (below) the main peak in the spin-down (up) spectral function decrease significantly as the Zeeman splitting is increased, then disappear when Δ exceeds the line-width of the Kondo peak which is proportional to the Kondo temperature

$k_B T_K$. However, for larger splitting, the main Kondo peak itself will be much suppressed, so that this spin-dependence of the Kondo phonon-satellites will not be resolved at all.

To understand how this pattern develops, it is helpful to recall that the satellite on different sides of the main peak is associated with different spin exchange process as depicted in figure 2. This peculiar pattern for finite Zeeman splitting indicates that the dominant contribution to the main peak in $A_\uparrow(\omega)$ comes from the coupling of the local state with the excited conduction electron states, while for $A_\downarrow(\omega)$ the dominant contribution comes from the coupling with the excited hole states. If $\Delta = 0$, as illustrated in figure 2, both spin exchange processes contribute to the Kondo main peak. When Δ starts to increase, both spin exchange processes decay in magnitude, but at different rates. When Zeeman splitting increases further, it would be possible that while one spin exchange process remains finite, the other is already totally suppressed. This results in the spin separation of the Kondo phonon-satellites in the spectral function. However, when $\Delta \gg k_B T_K$, both processes are unlikely to happen and finally the Kondo peaks are quenched.

The spin-down (up) spectral function for fixed Zeeman splitting is shown in figure 6(a) (figure 6(b)) as a function of ω and V_{bias}, in which the highlighting cross lines correspond to the Kondo satellites. Explicitly, the sections at the four typical bias voltages marked by the dashed lines in figures 6(a) and (b) are also plotted in figure 6(c). One can clearly see that, when the bias voltage turns on, each Kondo peak is separated into two sub-peaks related to two Fermi levels, respectively. These two sub-sets of Kondo satellites separate from each other further when V_{bias} increases, resulting in the peculiar pattern as shown in figure 6(c).

5. Conclusion

In summary, taking advantage of the improved treatment of the electron–phonon interaction and the extended equation of motion approach, we have systematically investigated the Kondo effect in the SMT in the presence of electron–phonon interaction, finite bias voltage, and Zeeman splitting. The Kondo phonon-satellites observed in recent SMT transport experiments [15–17] have been confirmed and explained by our results. Moreover, peculiar patterns of Kondo phonon-satellites in the spectral function as well as the differential conductance have also been predicted and explained by a clear physics picture. Although it is the interplay between the EPI and Kondo processes that is discussed here, the physics picture and the theoretical calculation presented here may also be applicable to some other cases. For instance, the interplay of electronic internal excitations and the Kondo processes can also manifest themselves in some parallel Kondo satellites [8].

Acknowledgments

The authors are grateful for helpful discussions with H Zhai, Z G Zhu, F Ye, C X Liu and R B Liu. This work is supported by the NSF of China (Grant Nos 10374056, 10574076), the MOE of China (Grant No 200221), and the Program of Basic Research Development of China (Grant No 2001CB610508).

References

[1] Ng T K and Lee P A 1988 *Phys. Rev. Lett.* **61** 1768
[2] Glazman L I and Raikh M E 1988 *JETP Lett.* **47** 452
[3] Hewson A C 1997 *The Kondo Problem to Heavy Fermions* (Cambridge: Cambridge University Press)
[4] Cronenwett S M, Oosterkamp T H and Kouwenhoven L P 1998 *Science* **281** 540

[5] Gordon D G, Shtrikman H, Mahalu D, Magder D A, Meirav U and Kastner M A 1998 *Nature* **391** 156
[6] Schmid J, Weis J, Eberl K and Klitzing K v 1998 *Physica* B **256** 182
[7] Wiel W G v d, Franceschi S D, Fujisawa T, Elzerman J M, Tarucha S and Kouwenhoven L P 2000 *Science* **289** 22
[8] Nygård J, Cobden D H and Lindelof P E 2000 *Nature* **408** 342
[9] Park J, Pasupathy A N, Goldsmith J I, Chang C, Yalsh Y, Petta J R, Rinkoskl M, Sethna J P, Abruña H D, McEuen P L and Ralph D C 2002 *Nature* **417** 722
[10] Liang W, Shores M P, Bockrath M, Long J R and Park H 2002 *Nature* **417** 725
[11] Pasupathy A N, Bialczak R C, Martinek J, Grose J E, Donev L A K, McEuen P L and Ralph D C 2004 *Science* **306** 86
[12] Kogan A, Amasha S and Kastner M A 2004 *Science* **304** 1293
[13] Martinek J, Utsumi Y, Imamura H, Barnaś J, Maekawa S, Köning J and Schön G 2003 *Phys. Rev. Lett.* **91** 127203
[14] Choi M S, Sanchez D and López R 2004 *Phys. Rev. Lett.* **92** 056601
[15] Yu L H and Natelson D 2004 *Nano Lett.* **4** 79
[16] Yu L H and Natelson D 2004 *Nanotechnology* **15** S517
[17] Yu L H, Keane Z K, Ciszek J W, Cheng L, Stewart M P, Tour J M and Natelson D 2004 *Phys. Rev. Lett.* **93** 266802
[18] Park H, Park J, Lim A K L, Anderson E H, Alivisatos A P and McEuen P L 2000 *Nature* **407** 57
[19] Koch J and Oppen F V 2005 *Phys. Rev. Lett.* **94** 206804
[20] Galperin M, Ratner M A and Nitzan A 2004 *Nano Lett.* **4** 1605
[21] Chen Z Z, Lü R and Zhu B F 2005 *Phys. Rev.* B **71** 165324
[22] Yosida K 1966 *Phys. Rev.* **147** 223
[23] Mahan G D 1990 *Many-Particle Physics* 2nd edn (New York: Plenum) p 967
[24] Köning J, Schoeller H and Schön G 1996 *Phys. Rev. Lett.* **76** 1715
[25] Köning J, Schmid J and Schoeller H 1996 *Phys. Rev.* B **54** 16820
[26] Hewson A C and Meyer D 2002 *J. Phys.: Condens. Matter* **14** 427
[27] Cornaglia P S, Ness H and Grempel D R 2004 *Phys. Rev. Lett.* **93** 147201
[28] Cornaglia P S, Grempel D R and Ness H 2005 *Phys. Rev.* B **71** 075320
[29] Cornaglia P S and Grempel D R 2005 *Phys. Rev.* B **71** 245326
[30] Paaske J and Flensberg K 2005 *Phys. Rev. Lett.* **94** 176801
[31] Lee H C and Choi H Y 2004 *Phys. Rev.* B **70** 085114
[32] Aji V, Moore J E and Varma C M 2003 *Preprint* cond-mat/0302222
[33] Han J H 2004 *Preprint* cond-mat/0405477
[34] Mitra A, Aleiner I and Millis A J 2004 *Preprint* cond-mat/0409248
[35] Kubatkin S, Danilov A, Hjort M, Cornil J, Brédas J L, Stuhr-Hansen N, Hedegård P and Bjornholm T 2003 *Nature* **425** 698
[36] Lundin U and McKenzie R H 2002 *Phys. Rev.* B **66** 075303
[37] Kuo D M T and Chang Y C 2002 *Phys. Rev.* B **66** 085311
[38] Zhu J X and Balatsky A V 2003 *Phys. Rev.* B **67** 165326
[39] Mahan G D 1990 *Many-Particle Physics* 2nd edn (New York: Plenum) p 533
[40] Hewson A C and Newns D M 1979 *J. Phys. C: Solid State Phys.* **12** 1665
[41] Hewson A C and Newns D M 1980 *J. Phys. C: Solid State Phys.* **13** 4477
[42] Meir Y, Wingreen N S and Lee P A 1993 *Phys. Rev. Lett.* **70** 2601
[43] Świrkowicz R, Barnaś J and Wilczyński M 2003 *Phys. Rev.* B **68** 195318
[44] Lacroix C 1981 *J. Phys. F: Met. Phys.* **11** 2389
[45] Huag H and Jauho A P 1998 *Quantum Kinetics in Transort and Optics of Semiconductors* (New York: Springer)
[46] Kashcheyevs V, Aharony A and Wohlman O E 2006 *Phys. Rev.* B **73** 125338
[47] Ng T K 1996 *Phys. Rev. Lett.* **76** 487
[48] Meir Y and Wingreen N S 1992 *Phys. Rev. Lett.* **68** 2512
[49] Jauho A-P, Wingreen N S and Meir Y 1994 *Phys. Rev.* B **50** 5528
[50] Appelbaum J 1966 *Phys. Rev.* **17** 91